

Fault-tolerance of $[[6, 1, 3]]$ non-CSS code family generated using measurements on graph states

Harsh Gupta*, Pranav Maheshwari† and Ankur Raina‡

*‡Department of EECS, Indian Institute of Science Education and Research Bhopal, India

†Department of Physics, Indian Institute of Science Education and Research Pune, India

Email: *harsh22@iiserb.ac.in, †pranav.maheshwari@students.iiserpune.ac.in, ‡ankur@iiserb.ac.in

Abstract—We construct and analyze the fault tolerance of $[[6, 1, 3]]$ non-CSS quantum error correcting code under the anisotropic and depolarizing noise models. This rate-optimized code achieves fault-tolerance using a single ancilla qubit for syndrome measurement under anisotropic noise conditions. This method was called fault-tolerance using bare ancilla by Brown *et al.* We give explicit construction of the code using measurements on non-planar graph states. We also argue that using our approach, we can construct a family of such fault-tolerant codes. This method fills a notable gap in constructing fault-tolerant non-CSS code families.

I. INTRODUCTION

Quantum systems are advancing rapidly and exhibit increased sensitivity to their environments. In quantum computation, operations on qubits must be executed without errors to ensure the accuracy of the results. Consequently, developing an effective Quantum Error Correcting Code (QECC) is essential to facilitate reliable computation. Implementing QECCs in practical scenarios presents significant challenges, with fault tolerance being a major bottleneck. Calderbank-Shor-Steane (CSS) codes are notable within the extensively studied families of quantum error-correcting codes due to their ability to rectify Pauli X and Pauli Z errors using purely X and Z type stabilizers [1]. In the CSS family, the minimum number of physical qubits required to encode the information of one logical qubit is seven [1]. Adding a layer of fault tolerance further increases the number of qubits required. One of the earliest codes tested for fault tolerance on small systems is the $[[4, 2, 2]]$ QECC [2], [3]. This code only detects a Pauli error as its minimum distance is two. Any limited error-correcting capacity of a QECC imposes significant resource overhead required for fault-tolerant (FT) quantum computation.

While performing a computation, fault-tolerance can be achieved if the error rate is below a certain threshold [4], [5]. Various methods exist for fault-tolerant syndrome extraction [6]. Steane’s method requires an FT logical state in the syndrome measurement, whereas Shor’s method requires extra qubits prepared in the cat state for FT syndrome measurement [7], [8]. Similarly, Knill’s method [9] uses a logical Bell pair for syndrome extraction. It is possible to make the $[[5, 1, 3]]$ code fault-tolerant with eight qubits and the $[[7, 1, 3]]$ code fault-tolerant with nine qubits as suggested by Yoder and Kim [10]. Brown *et al.* proposed a scheme for syndrome extraction on a $[[7, 1, 3]]$ non-CSS code using only one ancillary qubit [11]. By cleverly permuting the order

of gates, correcting any error propagating from the ancilla qubit to the data qubit is possible. In [12], the authors used the permutation technique of [13] to show fault tolerance in $[[8, 1, 3]]$ non-CSS code with the calculation of promising pseudo-thresholds.

In this paper, we present a rate-optimized $[[6, 1, 3]]$ non-CSS code for which FT syndrome extraction is possible. We also present a scheme for generating a family of such codes that can use the technique of permutation of gates presented in [12], [13] to demonstrate FT syndrome extraction. We call this family of codes as *bare codes*. Our approach utilizes the knowledge of parity check matrix and measurements on graph states [14], [15], [16], [17] to generate the bare code family. Our method identifies the connection between graph state codes and bare codes. FT syndrome extraction can be performed using bare codes under the anisotropic and depolarizing noise models. The decoder uses a look-up table to detect and correct all single-qubit errors. We manually populate the table with entries for the two-qubit errors that occur by error propagation during syndrome measurement. In this way, we are also able to correct those propagation errors.

The paper is organized as follows: The $[[6, 1, 3]]$ code is presented in Section II, where we discuss fault-tolerant syndrome extraction under noise models of interest. Section III presents a measurement-based scheme for finding a family of such $[[6, 1, 3]]$ codes. Simulations depicting the logical error rates for this code are presented in Section IV with the conclusion in Section V.

II. FAULT TOLERANT $[[6, 1, 3]]$ GRAPH CODE

Stabilizer formalism is a group theoretic approach to describe the $[[n, k, d]]$ QECC in an operator theoretic way [18]. Consider the n -fold tensor product of Pauli operators:

$$\mathcal{G}_n = \{\{\pm 1, \pm i\} \times \{I, X, Y, Z\}^{\otimes n}\}.$$

which is closed under multiplication. An Abelian subgroup of \mathcal{G}_n is called a stabilizer \mathcal{S} defined as

$$\mathcal{S} = \{g | g \neq -I, g \in \mathcal{G}_n, \forall i, j, [g_i, g_j] = 0\}.$$

Since \mathcal{S} is an Abelian group, it is possible to identify a 2^k dimensional vector space V_s that forms the codespace of an $[[n, k, d]]$ QECC. V_s is the linear span of the shared eigenvectors of \mathcal{S} , all simultaneously having an eigenvalue $+1$.

Such a stabilizer group \mathcal{S} can be described using its generators g_1, g_2, \dots, g_{n-k} as

$$\mathcal{S} = \langle g_1, g_2, \dots, g_{n-k} \rangle.$$

Stabilizer codes are extensively studied, with fault-tolerance being an active area of research [5]. FT syndrome extraction is a cog in the wheel of fault-tolerant quantum computation.

FT syndrome extraction with one ancillary qubit was first analyzed by Brown *et al.* They showed that a $[[7, 1, 3]]$ non-CSS code is capable of exhibiting fault-tolerance under the anisotropic error model [11]. For the depolarizing error model, fault-tolerance of the same code using an additional flag qubit was shown by Chao and Reichardt [13]. Building on the above ideas, fault-tolerance of the $[[8, 1, 3]]$ non-CSS QECC was shown in [12] under the anisotropic and depolarizing error models. In addition, pseudo-thresholds were calculated for these noise models.

We know that the smallest QECC of distance three, i.e., $[[5, 1, 3]]$ cannot be FT with the above scheme of one ancillary qubit in syndrome measurement. This is because the code is exhausted of syndromes for all single-qubit errors. Therefore, the existence of the $[[6, 1, 3]]$ code as the most rate-efficient FT code with one ancillary qubit in the syndrome measurement is strongly anticipated. We introduce the $[[6, 1, 3]]$ non-CSS fault-tolerant QECC using the principle of fault-tolerance with one ancillary qubit calling it a *bare code* as described in Section II-A. Furthermore, in Section III, we delineate the algorithmic framework for identifying such codes and provide the explicit construction methodology for FT codes using measurements on graph states.

A. $[[6, 1, 3]]$ FT code

The elements of the stabilizer group \mathcal{S} are also called stabilizers in popular literature. In this paper, we also use the same representation. Let us consider the stabilizers of the $[[6, 1, 3]]$ code in our study:

$$\mathcal{S}_6 = \langle Z_0 X_1 Z_2 Z_4 Z_5, Z_0 Z_1 X_2 Z_4 Z_5, Y_0 Z_1 Z_2 Y_3 Z_5, X_0 Z_3 X_4 Z_5, Z_1 Z_2 Z_3 Z_4 X_5 \rangle. \quad (1)$$

The corresponding logical operators are :

$$\begin{aligned} \text{logical } \bar{X} &: Z_0 X_3 Z_5 \\ \text{logical } \bar{Z} &: Z_0 Z_3 Z_4 \end{aligned} \quad (2)$$

Stabilizers detect the occurrence of errors that anti-commute with them. Every error is associated with an n -bit binary tuple called as the syndrome which identifies the error. Table I shows the syndromes of all single-qubit errors that the $[[6, 1, 3]]$ code is capable of detecting and correcting. During syndrome measurement, failure of two-qubit gates between data and ancilla qubit leads to errors in the quantum circuit. There are two types of error that we are considering for the $[[6, 1, 3]]$ FT code: the single qubit in ancilla qubit and the two-qubit error between ancilla qubit and data qubit. Error in the data qubit during syndrome measurement, which helps to propagate error in other data qubits called as hook error [19]. Sometimes, hook error leads to logical error, which makes QECC vulnerable.

Error	Syndrome	Error	Syndrome	Error	Syndrome
Z_0	00110	X_0	11100	Y_0	11010
Z_1	10000	X_1	01101	Y_1	11101
Z_2	01000	X_2	10101	Y_2	11101
Z_3	00100	X_3	00111	Y_3	00011
Z_4	00010	X_4	11001	Y_4	11011
Z_5	00001	X_5	11110	Y_5	11111

Table I: Syndrome table for the $[[6, 1, 3]]$ bare code, showing the syndromes for all single qubit errors. The table includes seventeen unique syndromes, with Y_1 , and Y_2 , sharing the same syndrome.

1) *Single qubit error*: $P \otimes I$ error mimics the single qubit error in ancilla qubit and no error in data qubit, respectively, where $P = \{X, Y, Z\}$. Since the $Z \otimes I$ is commutative with both two-qubit gates as illustrated in Figure 1, Z error in the ancilla qubit does not propagate to the data qubit. Either Pauli

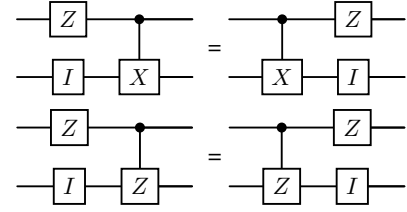


Figure 1: Pauli Z commutative with control- Z and control- X gate.

X or Y error in ancilla qubit leads to the error propagation to data qubits. Figure 2 shows various instances of how Pauli X error occurring on the ancilla qubit propagates in the course of syndrome measurement of the stabilizers of the $[[6, 1, 3]]$ code. For instance, consider only X error occurs in ancilla qubit after the two-qubit gate (red) between ancilla qubit and data qubit (q_2). Due to this, an error, i.e., $Y_3 Z_5$ propagates from the ancilla qubit to the data qubit whose syndrome is equivalent to that of Z_4 . On applying the correction of

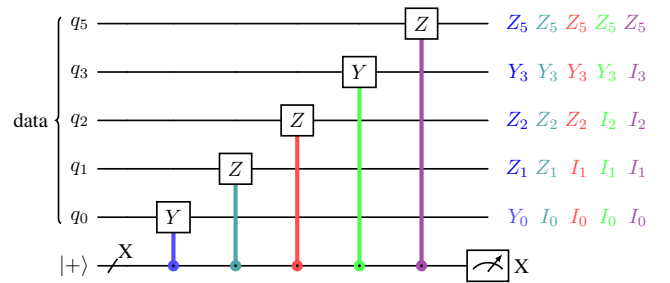


Figure 2: Propagation of errors into data qubits due to Pauli X error in the ancilla qubit at various locations while measuring the stabilizer $Y_0 Z_1 Z_2 Y_3 Z_4$. Each colour denotes where the error occurs in the ancilla qubit before that gate and the corresponding propagated error on data qubits.

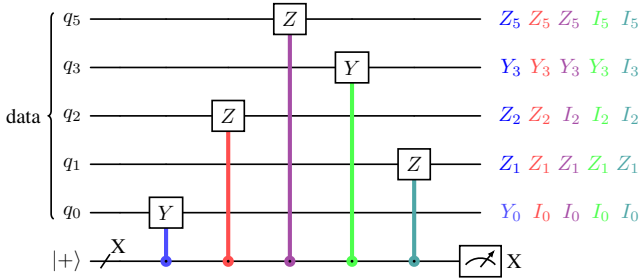


Figure 3: Measuring the syndrome of stabilizer $Y_0Z_1Z_2Y_3Z_4$ with the reordering of gates. Errors in ancilla qubit which propagates into errors in the data qubits lead to distinct syndromes.

Z_4 , we note that overall $Z_4Y_3Z_5$ gets applied on the data qubits, equivalent to the logical \bar{Y} error. The occurrence of this logical error can be circumvented by strategically rearranging the gates, as illustrated in Figure 3. If errors occur in the bare ancilla qubit after the two-qubit gate, the propagated errors have unique syndromes listed in Table II. Therefore, we can correct the error by applying the corresponding corrector operator preventing a logical error. A similar method is applied to other stabilizer measurements. This effectively prevents the occurrence of logical errors on data qubits due to the occurrence of errors on the bare ancilla qubit.

LOOK-UP TABLE with manual entries		
Syndrome	Error	Location
01110	Z_0Z_2	Bare ancilla error
01111	$Z_0Z_2Z_5$	Bare ancilla error
10111	X_2Z_4	Bare ancilla error
10001	$Z_0X_2Z_4$	Bare ancilla error
10010	Y_0Z_2	Bare ancilla error
10011	$Y_0Z_2Z_5$	Bare ancilla error
00101	X_0X_4	Bare ancilla error
10110	Z_2X_5	Bare ancilla error
10100	$Z_2Z_4X_5$	Bare ancilla error
01010	Z_2Z_4	Hook error
01011	$X_0X_2Z_3$	Hook error
01100	$Y_0Z_2X_5$	Hook error
01001	Z_2Z_5	Two qubit data error
11000	Z_1Z_2	Two qubit data error

Table II: Lookup table used in the correction of errors on the data qubits of the $[[6, 1, 3]]$ code.

2) *Two qubit error*: When two-qubit gates are employed, the error occurs between the ancilla and data qubit. $[[6, 1, 3]]$ is vulnerable due to two-qubit hook errors because sometimes it leads to logical errors after the correction step. For example, consider a two-qubit $Z \otimes X$ hook error shown in Figure 4. $Z \otimes X$ error transforms into $Z_3Z_4Z_5$ error on data qubits. The syndrome corresponding to $Z_3Z_4Z_5$ error is 00111, which

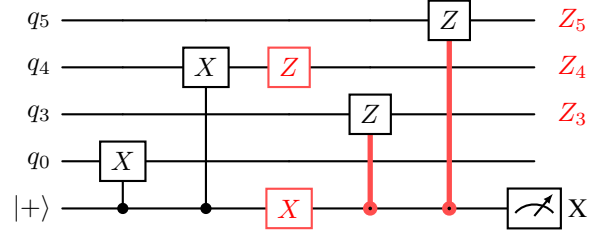


Figure 4: Due to hook errors, data qubits suffer from logical \bar{Y} errors.

Data Error	Syndrome	Data Error	Syndrome
$Z_0X_1Z_2Z_4Z_5 \rightarrow Z_0Z_2Z_5Z_4X_1$			
Z_0X_2	10011	Z_0Y_2	11011
Z_0Z_2	01110	$Z_0Z_2X_5$	10000
$Z_0Z_2Y_5$	10001	Z_4X_1	01111
Y_4X_1	10110	X_4X_1	10100
$Z_0Z_1X_2Z_4Z_5 \rightarrow Z_4X_2Z_0Z_5Z_1$			
Z_4X_2	10111	Z_4Y_2	11111
Z_4Z_2	01010	$Z_4X_2X_0$	01011
$Z_4X_2Y_0$	01101	Z_5Z_1	10001
Y_5Z_1	01111	X_5Z_1	01110
$Y_0Z_1Z_2Y_3Z_5 \rightarrow Y_0Z_2Z_5Y_3Z_1$			
Y_0X_2	01111	Y_0Y_2	00111
Y_0Z_2	10010	$Y_0Z_2X_5$	01100
$Y_0Z_2Y_5$	01101	Y_3Z_1	10011
Z_3Z_1	10100	X_3Z_1	10000
$X_0Z_3X_4Z_5 \rightarrow X_0X_4Z_3Z_5$			
X_0X_4	00101	X_0Y_4	00111
X_0Z_4	11110	Y_3Z_5	00010
X_3Z_5	00110	Z_5	00001
$Z_1Z_2Z_3Z_4X_5 \rightarrow X_5Z_2Z_4Z_3Z_1$			
X_5X_2	01011	X_5Y_2	00011
X_5Z_2	10110	$X_5Z_2X_4$	01111
$X_5Z_2Y_4$	01101	Z_3Z_1	10100
Y_3Z_1	10011	X_3Z_1	10111

Table III: Propagated errors in the $[[6, 1, 3]]$ code with their syndromes for the corresponding stabilizers. The rearranging of stabilizers is illustrated in grey boxes. The yellow coloured box represents the error generated by a fault in bare ancilla qubit. Red colour errors are logical errors due to hook errors, whereas black coloured errors are correctable.

is the same as that of a single-qubit X_3 error. Therefore, on applying the correction, the data qubits suffer from an overall logical error of $Y_3Z_4Z_5$. All the data errors mentioned in Table III in red are the results of hook errors which are converted into logical operators after correction.

A total of $2^{n-k} - 1 = 31$ non-zero five-bit tuples are available to detect the errors in data qubits. Out of these thirty-one, seventeen are utilized for single-qubit errors mentioned in Table I. We account for propagation errors arising from the ancilla qubit to the data qubits and manually assign nine syndromes as detailed in Table II. Three syndromes are

assigned for three specific hook errors and two syndromes are assigned for two random two-qubit data errors. Hence, the lookup table has been meticulously designed by manually associating each syndrome with specific errors.

Based on a single qubit and two-qubit errors, we consider depolarizing, and anisotropic noise models. Both models are thoroughly described in [12], [11], and we use the exact same definition to analyze the performance of the $[[6, 1, 3]]$ code.

As outlined in Section IV, the $[[6, 1, 3]]$ code demonstrates FT behaviour under anisotropic noise. Also, all the single qubit errors in the ancilla qubit are corrected due to unique syndromes generated for every corresponding Pauli error in the data qubits. This code demonstrates susceptibility to specific two-qubit error patterns, highlighting a limitation in its fault-tolerant capabilities. Using an additional flag qubit, the works in [10], [13] showed that it is possible to perform fault-tolerant syndrome measurement and account for all propagated errors. $[[7, 1, 3]]$ bare code considers a different ordering of the gates with flag qubits as compared to bare ancilla method [11]. The $[[6, 1, 3]]$ code considered in this paper can use the same ordering of gates to achieve fault-tolerant syndrome measurements for both methods, namely with a single bare ancilla and an additional flag. The method using a flag qubit leads to distinct syndromes after the measurement step as seen in Table III. For example, the circuit diagram for $X_0X_4Z_3Z_4$ stabilizer syndrome measurement using an additional flag qubit as shown in Figure 5.

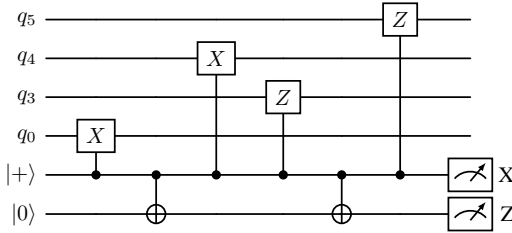


Figure 5: Syndrome measurement of the stabilizer $X_0X_4Z_3Z_5$ of the code $[[6, 1, 3]]$ using an additional flag. The same gate arrangement is used as that for the bare ancilla method.

The following section shows how to construct the non-CSS QECC codes that can demonstrate fault tolerant syndrome measurement under anisotropic noise models. We also find a distinct connection between these quantum codes, which are FT with a single ancillary qubit, and graph state codes. Using our approach, we find the $[[6, 1, 3]]$ FT code family consisting of some of the codes mentioned below

$$\begin{aligned}
\mathcal{S}_1 &= \langle Z_0Z_1X_2Z_4Z_5, Y_0Z_1Z_2Y_3Z_4, Y_0Z_1Z_3Y_4Z_5, \\
&\quad X_0X_1, Z_0Z_1Z_2Z_3X_5 \rangle, \\
\mathcal{S}_2 &= \langle X_0X_1Z_2Z_3Z_5, X_0Z_1Z_2X_3Z_4, Z_0Z_1Z_2X_4Z_5, \\
&\quad Z_0Z_2Z_3Z_4X_5, Y_0Y_2 \rangle, \\
\mathcal{S}_3 &= \langle X_1Z_2Z_3Z_4Z_5, Z_1X_2Z_3Z_4Z_5, X_0Z_1Z_2X_3Z_4, \\
&\quad Z_0Z_1Z_2X_4Z_5, Y_0Z_1Z_2Z_3Y_5 \rangle.
\end{aligned} \tag{3}$$

Additionally, we outline a systematic methodology for identifying FT codes specifically tailored to address the challenges posed by anisotropic and depolarizing noise models.

III. CONSTRUCTION OF FT CODES USING MEASUREMENTS

MBQC was introduced by Raussendorf *et al.*, which differs from other quantum computation models by leveraging measurements for quantum computation [20]. Starting with individual qubits, each prepared in $|+\rangle$ state and then connected these qubits with a controlled-phase gate (CZ). A network of interconnected qubits forms a specific type of entangled state known as a cluster state or a graph state. A graph state can be mathematically represented as an undirected graph $G = (V, E)$, where V denotes the set of vertices corresponding to the qubits, and E represents the edges indicating entanglement between the qubits. Figure 6 illustrates this graph-based representation of the planar two-dimensional cluster state.

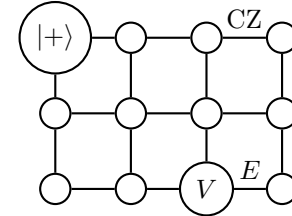


Figure 6: Cluster as graph $G = (V, E)$ where V is the set of vertices and E is the set of edges. Each edge corresponds to a CZ gate.

A. Encoding information using MBQC

Consider a graph state of n qubits described by a graph G . This graph state is described by the simultaneous $(+1)$ eigenspace of the elements of the Stabilizer group \mathcal{S}_G , namely g_0, g_1, \dots, g_{n-1} :

$$g_j = X_j \prod_{i \in \mathcal{N}_j} Z_i, j \in \{0, 1, \dots, n-1\}, \tag{4}$$

where \mathcal{N}_j denotes the neighbours of the node j . The entangled state resulting from the connections due to CZ gates is

$$|\psi\rangle = \prod_{(i,j) \in E} CZ_{ij} |+\rangle^{\otimes n} \tag{5}$$

Suppose a Pauli measurement is done on a single qubit of this graph state. Depending on the measurement outcome, the graph state gets projected onto a new state. Interestingly the post-measurement state can also be described by stabilizers. The rules to find the stabilizer generators of the post-measurement state can be found [5]. How the stabilizer group evolves for the graph state when subjected to different types of measurements is thoroughly described in [21], [22]. Consider a qubit having an arbitrary quantum state $|\phi\rangle$. We embed this information into a larger quantum system if this qubit is also connected to the graph state via CZ gates. We call this qubit whose quantum message is embedded into a graph state as the message qubit. Suppose a Pauli measurement is performed on

this message qubit. How the stabilizers evolve after measuring the message qubit can be seen in [23]. These works use the Heisenberg picture of the evolution of operators to evolve from stabilizer \mathcal{S}_G described by Eq. 4.

In this paper, we evolve the parity check matrix which is equivalent to the operator method. This matrix method is a new way of finding the evolved stabilizer set after measurement. For example, we observe that if we measure the message qubit of a graph state in the X basis the post-measurement state can be seen as a way of encoding to form interesting non-CSS QECCs. We call the remaining non-message qubits in the graph state as check qubits.

B. Matrix Method

Parity check matrix for a stabilizer code associated with $n + k$ qubits graph state includes k message qubits can be written in an elegant form as given below [24]:

$$\mathbf{H} = [\mathbf{I}_{n \times n} : \mathbf{0}_{n \times k} | \mathbf{A}_{n \times n}^{\text{cc}} : \mathbf{A}_{n \times k}^{\text{cm}}], \quad (6)$$

where $\mathbf{A}_{n \times n}^{\text{cc}}$ is an adjacency matrix associated with the check nodes (qubits without message input) of an $n + k$ qubit graph state. $\mathbf{A}_{n \times k}^{\text{cm}}$ matrix indicates the connection of the check nodes to the message nodes. $\mathbf{I}_{n \times n}$ is the identity matrix of order n and $\mathbf{0}_{n \times k}$ is the NULL matrix. We use non-planar graphs to generate the family of fault-tolerant non-CSS codes. Algorithm 1 describes how to get an encoded stabilizer using measurements on graph states. We use an example to describe the steps.

Algorithm 1: Stabilizer for the QECC using MBQC

Input: $\mathbf{H} = [\mathbf{I}_{n \times n} : \mathbf{0}_{n \times k} | \mathbf{A}_{n \times n}^{\text{cc}} : \mathbf{A}_{n \times k}^{\text{cm}}]$

Initialization:

1 Set $\text{var} = \text{NULL}$ and $k = 1$

Step1: Identify the first row with a 1 in the last column

2 **for** $i = 1$ to n **do**

3 **if** $\mathbf{H}[i][2n+2k] == 1$ **then**

4 Set $\text{var} = i$

Step2: Add that row whose $\text{pos} = \text{var}$ to all other rows in which the last column contains 1

5 **for** $j = 1$ to n **do**

6 **if** $j \neq i$ **and** $\mathbf{H}[j][2n+2k] == 1$ **then**

7 Add the row var to row j (element-wise mod two addition)

Step3: Deletion of rows and columns

8 Remove the $(n+k)$ and $2(n+k)$ position column from \mathbf{H}

9 Remove the row i (var) from \mathbf{H}

Output: \mathbf{H}' with dimension $n - k \times 2n$

C. Construction: $[[6, 1, 3]]$ FT QECC

For the construction of the $[[6, 1, 3]]$ FT QECC, we consider a seven-qubit graph state. The first six qubits, namely those

labelled 0 through 5, are prepared in the $|+\rangle$ state and seventh qubit, labelled 6 is the message qubit as seen in Figure 7.

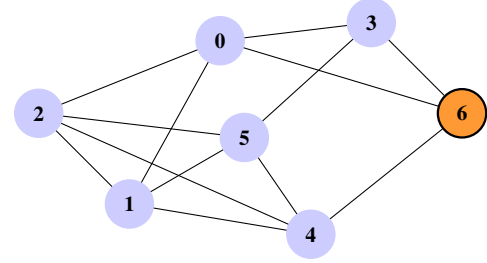


Figure 7: Seven qubit graph where one message qubit(orange) is measured in the X basis.

\mathcal{S}_7 is the stabilizer for the above graph state with generators

$$\mathcal{S}_7 = \langle X_0 Z_1 Z_2 Z_3 Z_6, Z_0 X_1 Z_2 Z_4 Z_5, Z_0 Z_1 X_2 Z_4 Z_5, Z_0 X_3 Z_5 Z_6, Z_1 Z_2 X_4 Z_5 Z_6, Z_1 Z_2 Z_3 Z_4 X_5 \rangle. \quad (7)$$

We use Algorithm 1 to show the changes in the parity check matrix once the message qubit is measured in the X basis. We note that the message qubit is numbered 6 and $\hat{\cdot}$ symbol is used where results are obtained after measurement. Consider the parity check matrix ($\mathbf{H} = [\mathbf{H}_x | \mathbf{H}_z]$) of the graph state:

$$\mathbf{H}_7 = \left[\begin{array}{cccccc|cccccc} 1 & 0 & 0 & 0 & 0 & 0 & 0 & 0 & 1 & 1 & 1 & 0 & 0 & 0 & 1 \\ 0 & 1 & 0 & 0 & 0 & 0 & 0 & 0 & 1 & 0 & 1 & 0 & 1 & 1 & 0 \\ 0 & 0 & 1 & 0 & 0 & 0 & 0 & 0 & 1 & 1 & 0 & 0 & 1 & 1 & 0 \\ 0 & 0 & 0 & 1 & 0 & 0 & 0 & 0 & 1 & 0 & 0 & 0 & 0 & 1 & 1 \\ 0 & 0 & 0 & 0 & 1 & 0 & 0 & 0 & 0 & 1 & 1 & 0 & 0 & 1 & 1 \\ 0 & 0 & 0 & 0 & 0 & 1 & 0 & 0 & 0 & 1 & 1 & 1 & 1 & 0 & 0 \end{array} \right]. \quad (8)$$

First row of the above matrix corresponds to the first stabilizer $X_0 Z_1 Z_2 Z_3 Z_6$ of the set \mathcal{S}_7 . This row is added with other rows corresponding to other stabilizers of the set \mathcal{S}_7 so that all the stabilizers commute with X_6 except $X_0 Z_1 Z_2 Z_3 Z_6$. We remove the seventh, fourteenth column and the first row from the matrix \mathbf{H}_7 because the message qubit is measured. Operations and the changes are mentioned below in Eq.(9):

$$\begin{aligned} & \left[\begin{array}{cccccc|cccccc} \hat{1} & \hat{0} & \hat{0} & \hat{0} & \hat{0} & \hat{0} & \hat{0} & \hat{0} & 0 & 1 & 1 & 1 & 0 & 0 & 0 \\ 0 & 1 & 0 & 0 & 0 & 0 & 0 & 0 & 1 & 0 & 1 & 0 & 1 & 1 & 0 \\ 0 & 0 & 1 & 0 & 0 & 0 & 0 & 0 & 1 & 1 & 0 & 0 & 1 & 1 & 0 \\ 1 & 0 & 0 & 1 & 0 & 0 & 0 & 0 & 1 & 0 & 0 & 0 & 0 & 1 & 0 \\ 1 & 0 & 0 & 0 & 1 & 0 & 0 & 0 & 0 & 1 & 1 & 0 & 0 & 1 & 0 \\ 0 & 0 & 0 & 0 & 0 & 1 & 0 & 0 & 0 & 1 & 1 & 1 & 1 & 0 & 0 \end{array} \right] \\ \Rightarrow \hat{\mathbf{H}}_6 &= \left[\begin{array}{cccccc|cccccc} 0 & 1 & 0 & 0 & 0 & 0 & 0 & 0 & 1 & 0 & 1 & 0 & 1 & 1 & 1 \\ 0 & 0 & 1 & 0 & 0 & 0 & 0 & 0 & 1 & 1 & 0 & 0 & 1 & 1 & 1 \\ 1 & 0 & 0 & 1 & 0 & 0 & 0 & 0 & 1 & 1 & 1 & 1 & 0 & 1 & 1 \\ 1 & 0 & 0 & 0 & 1 & 0 & 0 & 0 & 0 & 0 & 0 & 1 & 0 & 1 & 1 \\ 0 & 0 & 0 & 0 & 0 & 1 & 0 & 0 & 0 & 1 & 1 & 1 & 1 & 1 & 0 \end{array} \right]. \end{aligned} \quad (9)$$

The stabilizer generators of the above parity check are given in Eq. (10), which are the same as mentioned in Eq. (1) for the $[[6,1,3]]$ code:

$$\hat{\mathcal{S}}_6 = \langle Z_0 X_1 Z_2 Z_4 Z_5, Z_0 Z_1 X_2 Z_4 Z_5, Y_0 Z_1 Z_2 Y_3 Z_5, X_0 Z_3 X_4 Z_5, Z_1 Z_2 Z_3 Z_4 X_5 \rangle. \quad (10)$$

Thus, we are able to obtain FT $[[6, 1, 3]]$ code from the the graph state in Figure 7 by measuring the message qubit in the X basis.

D. Construction of graph from stabilizers of QECC

Consider a situation where certain non-CSS code stabilizers are given. What we would like to know is if it is possible to generate this stabilizer set by the method of measuring a message qubit embedded in a graph state. It is already proven that all the stabilizer codes have their equivalent graph codes and vice-versa [14] [15]. The method for constructing graphs that pose properties equivalent to its associated stabilizer code can be found in [16]. However, not all stabilizer codes can be converted from the parent graph because they need to satisfy the structure described in Eq. (6). We find for the code stabilizers of interest in this paper, it is indeed possible to find a parent graph state. The parent graph state consisting of the message qubit would be subjected to a Pauli X measurement converting the stabilizer set to a new set that stabilizes the bare codes considered in this paper. To explain the methodology in detail, consider figuring out its parent graph that leads to the stabilizer \mathcal{S} of $[[6, 1, 3]]$ code upon measurement. This is done using Algorithm 2.

Algorithm 2: $(n + 1)$ qubit graph construction from the $[[n, 1, d]]$ stabilizer code

Input: Parity check matrix of $[[n, 1, d]]$ QECC:

$$\mathbf{H} = [\mathbf{H}_x | \mathbf{H}_z]$$

Step1: Exchanging columns (swapping qubit) with modulo two-row operation convert \mathbf{H} into

$$\left[\mathbf{P}_{n-1 \times 1} : \mathbf{I}_{n-1 \times n-1} \mid \mathbf{c}_{n-1 \times 1} : \mathbf{A}_{n-1 \times n-1} \right]$$

Step2: Modify the matrix:

$$\left[\begin{array}{ccc|ccc} 1 & \mathbf{0}_{1 \times n-1} & 0 & 0 & \mathbf{c}_{1 \times n-1}^T & 1 \\ \mathbf{P}_{n-1 \times 1} & \mathbf{I}_{n-1 \times n-1} & \mathbf{0}_{n-1 \times 1} & \mathbf{c}_{n-1 \times 1} & \mathbf{A}_{n-1 \times n-1} & \mathbf{0}_{n-1 \times 1} \end{array} \right]$$

Step3: Convert the above matrix into the below form denoted by \mathbf{H}_c :

$$\left[\begin{array}{ccc|ccc} 1 & \mathbf{0}_{1 \times n-1} & 0 & 0 & \mathbf{c}_{1 \times n-1}^T & 1 \\ \mathbf{0}_{n-1 \times 1} & \mathbf{I}_{n-1 \times n-1} & \mathbf{0}_{n-1 \times 1} & \mathbf{c}_{n-1 \times 1} & \mathbf{A}'_{n-1 \times n-1} & \mathbf{P}_{n-1 \times 1} \end{array} \right]$$

Output: $\mathbf{H}_c = [\mathbf{I}_{n \times n} : \mathbf{0}_{n \times 1} \mid \mathbf{A}_{n \times n}^{cc} : \mathbf{A}_{n \times 1}^{cm}]$

E. Observations

It is observed that for both the codes explained in [12] and [11], the corresponding parent graph can be obtained using Algorithm 2. This means that both codes can be obtained using measurements on graph states. This observation leads us to search the $[[6, 1, 3]]$ FT code, an optimized one, with the help of measurements on parent graph states. We obtain many $[[6, 1, 3]]$ bare codes mentioned in Eq. (3). Similarly, we can construct many $[[7, 1, 3]]$ and $[[8, 1, 3]]$ codes similar to the bare codes analysed in [11]. We also hypothesize the

existence of connections between bare code stabilizers and the codes we obtain by measuring message qubits on graph states. In the next subsection, we propose finding the FT codes using measurements.

F. Search Protocol: For FT QECC

Initially, we take a n qubit graph without a message qubit. The parity check matrix of that graph is :

$$\tilde{\mathbf{H}} = [\mathbf{I}_{n \times n} \mid \mathbf{A}_{n \times n}^{cc}]. \quad (11)$$

Note that in Eq. (11) there is no $\mathbf{A}_{n \times k}^{cm}$ term because it denotes the connection of message qubit with the stated graph above. Similarly $\mathbf{0}_{n \times k}$ is not there which is corresponding term to $\mathbf{A}_{n \times k}^{cm}$. We source all graphs from [25] where connections of the check qubits with the message qubits are varied. It gives us the parity check matrix in $[\mathbf{I}_{n \times n} : \mathbf{0}_{n \times k} \mid \mathbf{A}_{n \times n}^{cc} : \mathbf{A}_{n \times k}^{cm}]$ form, referred to as the parent graph. After that, we follow the procedure described in Algorithm 1 to generate QECC. It is observed that if the number of connections is less than three, we never get distance-three codes after measuring the message qubit in the X basis. We modify the parity check matrix of the obtained QECC as mentioned below:

$$\mathbf{H}_{xyz} = [\mathbf{H}_x \mid \mathbf{H}_z \mid \mathbf{H}_x \oplus \mathbf{H}_z] \quad (12)$$

In distance three CSS codes, the syndrome of Y errors is always unique to the syndrome of X and Z errors. However, in non-CSS codes, it is not always true. Therefore \mathbf{H}_{xyz} matrix gives the total unique syndrome for a particular non-CSS QECC for a single qubit error. Also, \mathbf{H}_{xyz} matrix is useful while implementing Algorithm 3, which helps to find FT codes.

Algorithm 3 process each stabilizer, $g_i \in \mathcal{S}$ and generate a list containing the permutations of operators with corresponding syndrome list associated with that g_i . The algorithm initializes through finding syndromes for each permutations of g_i which $\notin \mathbf{H}_{xyz}$ such that $\text{weight}(g_i) \geq 3$ and weight of permuted elements are $\text{weight}(g_i) - 2$. Note that each permutation element is further processed by substituting the last operator with P , where $P \in \{X, Y, Z\}$. It is a recursive process where we record the syndrome for each permutation element and compile a list of associated syndromes until the element's weight diminishes to one. Selected each element together with its matching syndrome list related to g_i , ensuring that the syndrome lists of all selected elements across stabilisers are unique. Picked each element with its associated syndrome list corresponding to g_i such that the syndrome list of all chosen elements across stabilizers is distinct. The selected operator sets form the FT code.

All codes referenced in Eq (3) were generated using Algorithm 3 from corresponding graph states depicted in Figure 8. In the next section, we simulated and analysed the FT $[[6, 1, 3]]$ bare code.

IV. SIMULATION AND ANALYSIS

The error correction analysis employs the method outlined in [12]. It consists of an encoder circuit, a detector circuit

Algorithm 3: Find Combination lists of stabilizers

Input:

1 Stabilizer set: $\mathcal{S} = \{g_1, g_2, \dots, g_n\}$

2 Modified parity check matrix:

$$\mathbf{H}_{xyz} = [\mathbf{H}_x | \mathbf{H}_z | \mathbf{H}_x \oplus \mathbf{H}_z]$$

Initialization:

3 stablist = [], comblist = [],
combsynlist = []

4 $w(S)$:= A function that calculates the weight of subset
 $S \subseteq \mathcal{S}$

5 $\text{syn}(S)$:= A function that calculates syndrome of
subset $S \subseteq \mathcal{S}$
Step1: Updated stabilizer list

6 for g_i in \mathcal{S} do
7 if $w(g_i) \geq 3$ then
8 stablist $\leftarrow g_i$
Step2: Combination set list for each g_i

9 for j in stablist do
 Initialization: clist = [], sclist = [],
 synlist = [], scsynlist = []

Step1:

10 for each $SS \subseteq g_i$ do
11 if $w(SS) == w(g_i) - 2$ then
12 if $\text{syn}(SS) \notin \mathbf{H}_{xyz}$ then
13 • Replace the last operator in the SS
 with $P \in \{X, Y, Z\}$
14 if For each P , $\text{syn}(SS) \notin \mathbf{H}_{xyz}$ then
15 clist $\leftarrow SS$
16 synlist $\leftarrow \text{syn}(SS)$
Step2: Recursive reduction

17 for each $SC \subseteq C$ do
18 while $w(SC) \notin 1$ do
19 if $\text{syn}(SC) \notin \mathbf{H}_{xyz}$ then
20 • Replace the last operator in the SC
 with $P \in \{X, Y, Z\}$
21 if For each P , $\text{syn}(SC) \notin \mathbf{H}_{xyz}$ then
22 sclist $\leftarrow SC$,
23 scsynlist $\leftarrow \text{syn}(SC)$
24 comblist[j] \leftarrow sclist
25 combsynlist[j] \leftarrow scsynlist

Output: List of permutations of operators for each
 $g_i \in \mathcal{S}$ together with the corresponding
syndrome list that are not included in \mathbf{H}_{xyz}

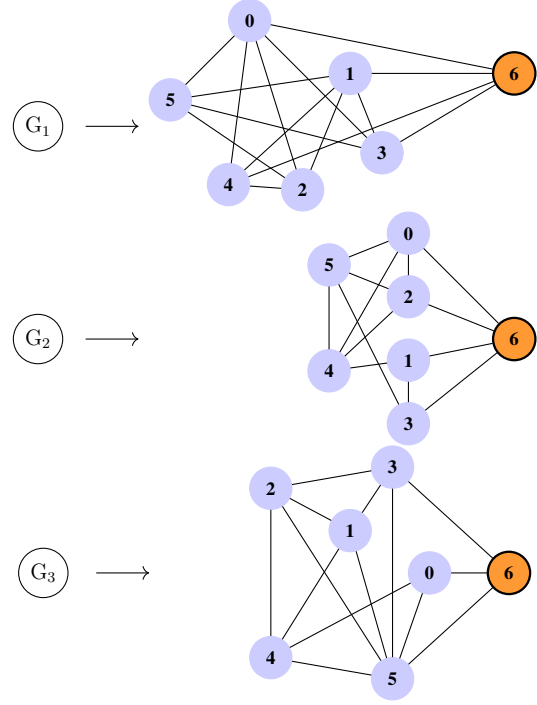


Figure 8: Graph states of seven qubits with one message qubit(orange). Every G_i graph state is corresponds to the $[[6, 1, 3]]$ FT bare codes denoted by \mathcal{S}_i mentioned in Eq. (3). After measuring the message qubit of every graph state (G_i) in X basis corresponding stabilizer set (\mathcal{S}_i) will be obtained.

A. Simulations

We use the simulation technique outlined in [12]. The encoder employs the stabilizer set derived from the method of measuring parent graph states. The detector comprises a combination of gates for each stabilizer in the order specified in Table III. The corrector uses an updated lookup table that maps syndromes to respective errors as mentioned in Table I and Table II.

We consider the noise in quantum gates only after encoding. The noise model is robust enough and considers all prominent errors such as state preparation, single-qubit, two-qubit, and readout errors, all with the same probability p of physical error rate. No noise is assumed in the quantum gates used in the corrector circuit. Error analysis simulations are performed using QISKIT [26], and all the codes are generated with the help of Python programs. We use the modified scheme where an error-free Detector and Corrector are placed in the end again before the (Encoder) † operation. For robust results, the circuit is executed 10^6 times for each value of the physical error rate for the anisotropic noise model. The above process is repeated for 5 rounds to obtain the range of results. For the depolarizing noise model, the circuit is executed 5×10^6 times for each value of the physical error rate, spanning with least value of 10^{-6} physical error rate. Again the above process is repeated for 5 rounds to obtain the range of results.

The logical error rate is calculated as the ratio of logical

for measuring stabilizer syndromes, and a corrector circuit that applies corrections based on the syndromes. Finally, the decoder, mathematically defined as the adjoint of the encoder, retrieves the message in the message qubit.

errors to the total number of circuit runs for each physical error rate. The mean, minimum, and maximum values from these 5 rounds are plotted against the physical error rate. Since we initialized the state in the logical zero state ($|0\rangle$), the logical \bar{Z} operator does not affect the encoded state. Consequently, only the logical \bar{X} and logical \bar{Y} operators are the logical errors that we can observe in measuring the final state after the decoder. As a result, the logical error rate is compared with $\frac{2}{3}p$ rather than p , where p is the physical error rate. The point at which the logical error rate cuts the unencoded error rate is the pseudo-threshold value indicating the value of the physical error rate below which the $[[6, 1, 3]]$ bare code is suitable. For easier visualization, we also compare physical error rates (p) to $\frac{1}{p^2}$ times the logical error rate. It gives the leading order coefficient of the probability of logical error. If the plot stabilizes, it ensures that the logical error rate is at least of order p^2 , which is less than an order of p below the threshold.

B. Results

From the above-described simulation scheme, the bare $[[6, 1, 3]]$ code provides promising pseudo-thresholds under the Anisotropic noise model. Figure 9 presents how logical error rates decrease with physical error rates.

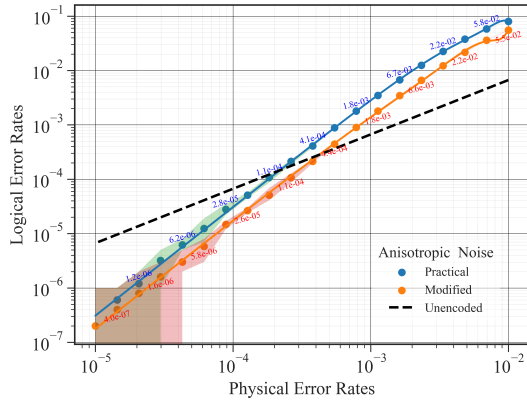


Figure 9: Logical rate of $[[6, 1, 3]]$ QECC for anisotropic noise. The modified version implies that the additional noise-free Detector and Corrector are applied at the end.

Figure 10 shows the incompetency of the code with the depolarizing noise. It is mainly due to the hook errors in the quantum circuit. And there are very few syndromes in $[[6, 1, 3]]$ code for which we can correct the hook errors generated because of the faults in the ancilla qubit. With the help of the flag method, which consists of an additional flag qubit, we will get a better logical rate. Due to logistic constraints, we did not employ the flag method in this code. However, we can see that with the help of a modified approach, we can find the pseudo-threshold.

Figure 11 presents the leading order of error rates, which stabilizes near the pseudo-threshold, proving the definitive improvement offered by the fault-tolerant structure of the code.

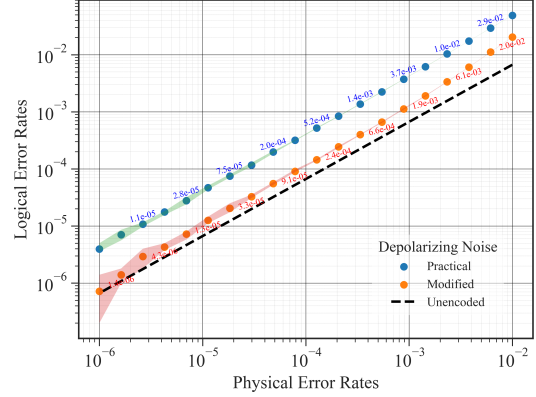


Figure 10: Logical rate of $[[6, 1, 3]]$ QECC for depolarizing noise. The logical error rate remains parallel to the physical error rate, but we can almost achieve a pseudo-threshold value with the extra noise-free Detector and Corrector.

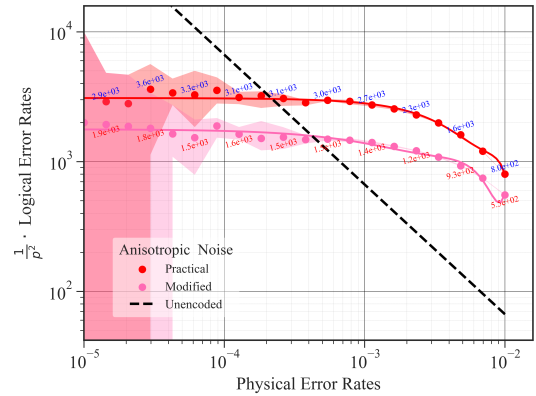


Figure 11: Leading orders of anisotropic noise - For $[[6, 1, 3]]$ bare code physical error rates (p) are mapped against $\frac{1}{p^2}$ times the logical error rate. The plot is stabilized which ensures that the order of logical error rate is at least of order p^2 , which is less than an order of p below the threshold

Table IV summarizes the obtained values of pseudo-thresholds and the leading orders based on best-fit curves. The leading order trend for p^2 in Figure 12 shows that the curve is not following the expected trend as seen in Figure 11 when physical error rates (p) is plotted against the $\frac{1}{p^2}$ times the logical error rate.

C. Analysis

We obtain a robust pseudo-threshold of 2×10^{-4} , which is the same as obtained for bare $[[7, 1, 3]]$ non-CSS code under anisotropic noise model [11]. The $[[6, 1, 3]]$ code also has better pseudo-threshold than $[[8, 1, 3]]$ bare fault tolerant code using the modified approach for anisotropic noise [12]. We did not get the pseudo-threshold for the depolarizing noise as seen in Figure 10. We observe that in this code, the modified approach provides better results than the practical one, as in

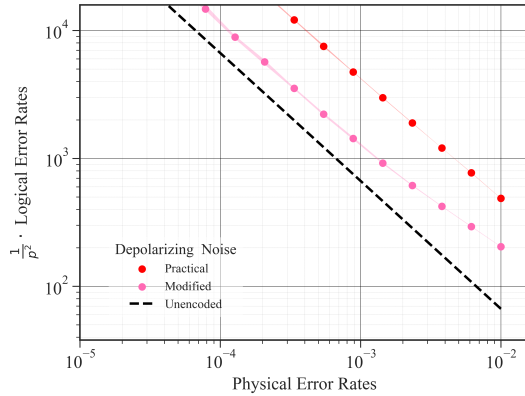


Figure 12: Leading orders of depolarizing noise- Here physical error rates (p) of $[[6, 1, 3]]$ bare code are mapped against $\frac{1}{p^2}$ times the logical error rate. The plot shows that the observed error rate almost parallels physical error rates (p) and does not stabilise order p^2 for the plotted given range.

Error Rates	Pseudo-thresholds	Leading Orders
Practical Approach	0.0002192	3092
Modified Approach	0.0004225	1774

Table IV: Metrics for anisotropic noise model

simulation, the code is left with many single-qubit errors, which are corrected when a noise-free detector and corrector circuit are applied. As a result, a very high logical error rate would be drastically reduced after correcting the single qubit errors, which the code can inherently correct.

V. CONCLUSION

This paper presents a family of rate-optimized $[[6, 1, 3]]$ QECC with fault-tolerant syndrome measurement done using one ancillary qubit. The code exhibits suboptimal performance under depolarizing noise due to the limited availability of syndromes to identify hook errors. We demonstrate a matrix method to find graph states that can be used to generate a family of non-CSS codes that can show fault tolerance. This approach enables a deeper understanding of the relationship between previously discovered FT codes and MBQC requiring further analysis.

VI. ACKNOWLEDGEMENTS

The authors thank Mainak Bhattacharyya for his valuable suggestions in preparing this manuscript and for his helpful suggestions regarding the Python code implementation. HG thanks IISER Bhopal for the institute doctoral fellowship.

REFERENCES

- [1] A. M. Steane, "Simple quantum error-correcting codes," *Phys. Rev. A*, vol. 54, pp. 4741–4751, Dec 1996. [Online]. Available: <https://link.aps.org/doi/10.1103/PhysRevA.54.4741>
- [2] C. Vuillot, "Is error detection helpful on ibm 5q chips?" *Quantum Info. Comput.*, vol. 18, no. 11–12, p. 949–964, Sep. 2018.
- [3] M. Takita, A. W. Cross, A. D. Córcoles, J. M. Chow, and J. M. Gambetta, "Experimental demonstration of fault-tolerant state preparation with superconducting qubits," *Phys. Rev. Lett.*, vol. 119, p. 180501, Oct 2017. [Online]. Available: <https://link.aps.org/doi/10.1103/PhysRevLett.119.180501>
- [4] D. Aharonov and M. Ben-Or, "Fault-tolerant quantum computation with constant error," in *Proceedings of the Twenty-Ninth Annual ACM Symposium on Theory of Computing*, ser. STOC '97. New York, NY, USA: Association for Computing Machinery, 1997, p. 176–188. [Online]. Available: <https://doi.org/10.1145/258533.258579>
- [5] M. Nielsen and I. Chuang, *Quantum Computation and Quantum Information: 10th Anniversary Edition*. Cambridge University Press, 2010. [Online]. Available: <https://books.google.co.in/books?id=s4DEy7o-a0C>
- [6] K. Fujii, "Quantum computation with topological codes: from qubit to topological fault-tolerance," 2015. [Online]. Available: <https://arxiv.org/abs/1504.01444>
- [7] A. M. Steane, "Active stabilization, quantum computation, and quantum state synthesis," *Phys. Rev. Lett.*, vol. 78, pp. 2252–2255, Mar 1997. [Online]. Available: <https://link.aps.org/doi/10.1103/PhysRevLett.78.2252>
- [8] D. P. DiVincenzo and P. W. Shor, "Fault-tolerant error correction with efficient quantum codes," *Phys. Rev. Lett.*, vol. 77, pp. 3260–3263, Oct 1996. [Online]. Available: <https://link.aps.org/doi/10.1103/PhysRevLett.77.3260>
- [9] E. Knill, "Quantum computing with realistically noisy devices," *Nature*, vol. 434, no. 7029, pp. 39–44, Mar 2005. [Online]. Available: <https://doi.org/10.1038/nature03350>
- [10] T. J. Yoder and I. H. Kim, "The surface code with a twist," *Quantum*, vol. 1, p. 2, Apr. 2017. [Online]. Available: <https://doi.org/10.22331/q-2017-04-25-2>
- [11] M. Li, M. Gutiérrez, S. E. David, A. Hernandez, and K. R. Brown, "Fault tolerance with bare ancillary qubits for a $[[7,1,3]]$ code," *Phys. Rev. A*, vol. 96, p. 032341, Sep 2017. [Online]. Available: <https://link.aps.org/doi/10.1103/PhysRevA.96.032341>
- [12] P. Maheshwari and A. Raina, "Fault-tolerance of the $[[8, 1, 3]]$ non-css code," in *2024 IEEE International Symposium on Information Theory Workshops (ISIT-W)*, 2024, pp. 1–6. [Online]. Available: <https://ieeexplore.ieee.org/document/10591768>
- [13] R. Chao and B. W. Reichardt, "Quantum error correction with only two extra qubits," *Phys. Rev. Lett.*, vol. 121, p. 050502, Aug 2018. [Online]. Available: <https://link.aps.org/doi/10.1103/PhysRevLett.121.050502>
- [14] D. Schlingemann and R. F. Werner, "Quantum error-correcting codes associated with graphs," *Physical Review A*, vol. 65, no. 1, dec 2001. [Online]. Available: <https://doi.org/10.1103/PhysRevA.65.012308>
- [15] M. Van den Nest, J. Dehaene, and B. De Moor, "Graphical description of the action of local clifford transformations on graph states," *Phys. Rev. A*, vol. 69, p. 022316, Feb 2004. [Online]. Available: <https://link.aps.org/doi/10.1103/PhysRevA.69.022316>
- [16] C. Cafaro, D. Markham, and P. van Loock, "Scheme for constructing graphs associated with stabilizer quantum codes," *Physical Review A*, Apr. 2015. [Online]. Available: <https://telecom-paris.hal.science/hal-02287093>
- [17] D. Schlingemann, "Stabilizer codes can be realized as graph codes," 2001. [Online]. Available: <https://arxiv.org/abs/quant-ph/0111080>
- [18] D. Gottesman, "Stabilizer codes and quantum error correction," 1997. [Online]. Available: <https://arxiv.org/abs/quant-ph/9705052>
- [19] E. Dennis, A. Kitaev, A. Landahl, and J. Preskill, "Topological quantum memory," *Journal of Mathematical Physics*, vol. 43, no. 9, pp. 4452–4505, 09 2002. [Online]. Available: <https://doi.org/10.1063/1.1499754>
- [20] R. Raussendorf, D. E. Browne, and H. J. Briegel, "Measurement-based quantum computation on cluster states," *Phys. Rev. A*, vol. 68, p. 022312, Aug 2003. [Online]. Available: <https://link.aps.org/doi/10.1103/PhysRevA.68.022312>
- [21] A. Patil and S. Guha, "Clifford manipulations of stabilizer states: A graphical rule book for clifford unitaries and measurements on cluster states, and application to photonic quantum computing," 2023. [Online]. Available: <https://arxiv.org/abs/2312.02377>
- [22] M. Hein, J. Eisert, and H. J. Briegel, "Multiparty entanglement in graph states," *Phys. Rev. A*, vol. 69, p. 062311, Jun 2004. [Online]. Available: <https://link.aps.org/doi/10.1103/PhysRevA.69.062311>
- [23] Y. Hwang and J. Heo, "On the relation between a graph code and a graph state," 2015. [Online]. Available: <https://arxiv.org/abs/1511.05647>

- [24] P. J. Nadkarni, A. Raina, and S. G. Srinivasa, "Recovery of distributed quantum information using graph states from a node failure," in *2017 IEEE Globecom Workshops (GC Wkshps)*, 2017, pp. 1–6.
- [25] B. McKayt, "Collections of graphs." [Online]. Available: <https://users.cecs.anu.edu.au/~bdm/data/graphs.html>
- [26] A. Javadi-Abhari, M. Treinish, K. Krsulich, C. J. Wood, J. Lishman, J. Gacon, S. Martiel, P. D. Nation, L. S. Bishop, A. W. Cross, B. R. Johnson, and J. M. Gambetta, "Quantum computing with qiskit," 2024. [Online]. Available: <https://arxiv.org/abs/2405.08810>